Article

Unconventional superconductivity without doping in infinite-layer nickelates under pressure

Simone Di Cataldo [1] ✉, **Paul Worm**[1], **Jan M. Tomczak** [1,2], **Liang Si** [3] & **Karsten Held** [1]

High-temperature unconventional superconductivity quite generically emerges from doping a strongly correlated parent compound, often (close to) an antiferromagnetic insulator. The recently developed dynamical vertex approximation is a state-of-the-art technique that has quantitatively predicted the superconducting dome of nickelates. Here, we apply it to study the effect of pressure in the infinite-layer nickelate $Sr_xPr_{1-x}NiO_2$. We reproduce the increase of the critical temperature (T_c) under pressure found in experiment up to 12 GPa. According to our results, T_c can be further increased with higher pressures. Even without Sr-doping the parent compound, $PrNiO_2$, will become a high-temperature superconductor thanks to a strongly enhanced self-doping of the Ni $d_{x^2-y^2}$ orbital under pressure. With a maximal T_c of 100 K around 100 GPa, nickelate superconductors can reach that of the best cuprates.

Ever since the discovery of high-temperature superconductivity in $LaBaCuO_4$[1], understanding or even predicting new unconventional (not electron-phonon-mediated) superconductors and identifying the pairing mechanism has been the object of an immense research effort. A new opportunity for a more thorough understanding arose with the discovery of superconductivity in several infinite-layer nickelates $A_{1-x}B_xNiO_2$[2–7], where A = La, Nd, Pr, and B = Sr, Ca are different combinations of rare earths and alkaline-earths. These nickelates are at the same time strikingly similar to cuprates (for this reason theory predicted nickelate superconductivity 20 years before experiment[8]) but also decidedly different. This constitutes an ideal combination to clarify the presumably common mechanism behind superconductivity in both systems. Superconductivity in nickelates was found to be quite independent of the rare earth A and dopant B[9] with a dome-like shape characteristic of unconventional superconductors.

Theoretical work has left little doubt that nickelates are, indeed, unconventional superconductors[10–12], and the similarity to the crystal and electronic structure of cuprates is striking[8,13]. There are, however, subtle differences between cuprates and nickelates: Compared to Cu^{2+}, the 3d bands of Ni^{1+} are separated by a larger energy from the oxygen ones, hence hybridization is weaker and oxygen plays a less prominent role than in cuprates. On the other hand, the rare-earth A-derived bands cross the Fermi level in nickelates and form electron pockets. These electron pockets self-dope the Ni $d_{x^2-y^2}$ band with about 5% holes[12,14–20] and prevent the parent compound from being an antiferromagnetic insulator. Given the inherent difficulty in incorporating the effect of strong electronic correlations, different theory groups have arrived at a variety of models for describing nickelates[16,19–26].

Based on a minimal model consisting of a 1-orbital Hubbard model for the Ni $d_{x^2-y^2}$ band[12] plus largely decoupled electron pockets, that only act as electron reservoirs, Kitatani et al.[20] accurately predicted the superconducting dome in Sr-doped $NdNiO_2$[20] prior to experiment[4,4,27]. In particular, the agreement to more recent defect-free films[27] is excellent. This includes the quantitative value of T_c, the doping region of the dome, and the skewness of the superconducting dome, see ref. 28. Also pentalayer nickelates[7] seamlessly fit the results of Ref. 28. In Refs. 20,29 some of us pointed out that larger T_c's should be possible if the ratio of interaction to hopping, U/t, is reduced.

In a recent seminal paper, Wang et al.[30] reported a substantial increase of T_c in $Sr_xPr_{1-x}NiO_2$ (x = 0.18) films on a $SrTiO_3$ (STO) substrate from 18 to 31 K if a pressure of 12 GPa is applied in a diamond anvil cell. There are no indications of a saturation of the increase of T_c

[1]Institut für Festkörperphysik, Technische Universität Wien, 1040 Wien, Austria. [2]King's College London, London WC2R 2LS, UK. [3]School of Physics, Northwest University, Xi'an 710127, China. ✉e-mail: simone.dicataldo@uniroma1.it
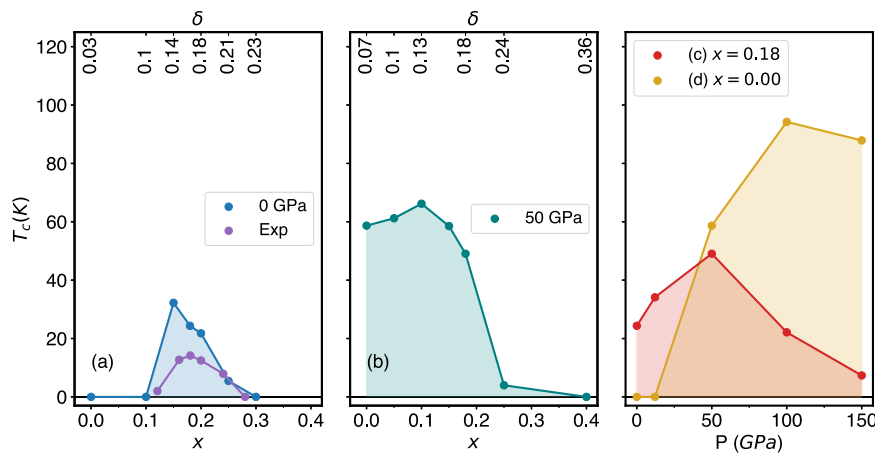
Fig. 1 | Phase diagram T_c vs. Sr-doping x and pressure P of Sr$_x$Pr$_{1-x}$NiO$_2$ as calculated in DΓA. Four different paths are considered: as a function of x for **a** 0 GPa and **b** 50 GPa; as a function of P at **c** $x = 0.18$ and **d** $x = 0$. The secondary (upper) x-axis of panels (**a**), **b** shows the effective hole doping δ of the Ni $d_{x^2-y^2}$ orbital with respect to half filling. Panel **a** also compares to the experimental result from ref. 58 (purple dots).

with pressure yet. First calculations of the electronic structure, fixing the in-plane lattice constant to the ambient pressure value and relaxing (reducing) the out-of-plane c-axis have been presented[31]. A large T_c under pressure[32] or at least a resistivity drop[33], has also been reported in another nickelate: La$_3$Ni$_2$O$_7$. With a $3d^{7.5}$ electronic configuration and prevalent charge density wave fluctuations, the mechanism in this compound is, however, clearly distinct from the (slightly doped) $3d^9$ nickelates considered here.

In this work, we employ the same state-of-the-art scheme that was successful in ref. 20, which is based on density functional theory (DFT), dynamical mean-field theory (DMFT), and the dynamical vertex approximation (DΓA). We study the pressure dependence of the superconducting phase diagram of PrNiO$_2$ (PNO) with and without Sr doping. We find (i) a strong increase of the hopping t, almost by a factor of two, when going from 0 to 150 GPa, while the value of U, obtained through constrained random-phase approximation (cRPA), remains essentially unchanged as in cuprates[34]. Importantly, pressure further results in (ii) deeper electron pockets, effectively increasing the hole doping δ of the Ni $d_{x^2-y^2}$ band with respect to half-filling. Altogether, this results in the phase diagrams shown in Fig. 1, the main result of our work. When going from (a) ambient pressure to (b) 50 GPa, T_c increases by up to a factor of two and d-wave superconductivity is observed in a much wider doping range—quite remarkably even without Sr doping. As a function of pressure, at doping fixed to $x = 0.18$ (c), the simulated phase diagram shows a very similar increase of T_c from 0 to 12 GPa as in experiment[30]. The figure further reveals that T_c will continue to increase up to 49 K at 50 GPa, followed by a rapid decrease at higher pressures. For the parent compound, PrNiO$_2$ ($x = 0$, d), the enhanced self-doping alone is sufficient to turn it superconducting with a maximum predicted T_c of close to 100 K at 100 GPa.

Results

As the superconducting nickelate films are grown onto an STO substrate, particular care has to be taken when simulating the effect of isotropic pressure in the diamond anvil cell (cf. Supplemental Material (SM) Section IA for a flowchart of the overall calculations and Section IC for further details of the pressure calculation). First, since the thickness of the film is 10–100 nm and thus negligible compared to that of the STO substrate, we calculate the STO equation of state in DFT and, from this, obtain the STO lattice parameters under pressure. Second, we fix the in-plane a (and b) lattice parameters to that of STO under pressure and find the lattice parameter c for the nickelate which minimizes the enthalpy at the given pressure. The resulting lattice

constants are shown in Table 1. This procedure reflects the response of the system to the rather isotropic pressures realized in the experiment whereas in ref. 31 the a–b lattice parameters had been fixed to that of unpressured STO[31].

With the crystal structure determined, we calculate the DFT electronic structure at pressures of 0, 12, 50, 100, and 150 GPa. Next, we perform a 10- and 1-orbital Wannierization around the Fermi energy, including all Pr-d plus Ni-d orbitals and only the Ni $d_{x^2-y^2}$ orbital, respectively. The DFT band structures and Wannier bands are shown in SM Fig. S5 and as white lines in Fig. 2.

Following the method of refs. 20,35, we supplement the Wannier Hamiltonian with a local intra-orbital Coulomb interaction of $U = 4.4$ eV (2.5 eV) and Hund's exchange $J = 0.65$ eV (0.25 eV) for Ni-$3d$ (Pr-$5d$) as calculated in cRPA in our previous work[36]. For the thus-derived 10-band model, we perform DMFT calculations. The resulting DMFT spectral function of undoped PNO is shown in Fig. 2, for 0 and 50 GPa. We see that the Ni $d_{x^2-y^2}$ orbital crossing the Fermi energy is strongly quasiparticle-renormalized compared to the DFT result (white lines). In addition, there are pockets at the Γ and A momenta, which essentially follow the DFT band structure without renormalization.

Important for the following is that, with the overall increase of bandwidth under pressure, the size of the pockets grows dramatically under pressure in DFT and DMFT alike. The enlargement of the Γ pocket can also be seen from the Fermi surface Fig. 2 (d) vs. (b). The effect at higher pressures is shown in SM Figs. S8 and S9.

The results of the 10-band model show that the low-energy physics of the system boils down to one-strongly correlated Ni $d_{x^2-y^2}$ orbital plus weakly correlated electron pockets. Here, the A-pocket does not hybridize by symmetry with the Ni $d_{x^2-y^2}$ band, as is evident by the mere crossing of both between R and A. The band forming the Γ

Table 1 | Ab initio values for the lattice constants and the hoppings of the 1-orbital Hubbard model for PrNiO$_2$ under pressure

P	a	c	t	t'	t''
[GPa]	[Å]	[Å]	[eV]	[eV]	[eV]
0	3.90	3.32	−0.39	0.10	−0.05
12.1	3.83	3.20	−0.42	0.10	−0.05
50	3.67	3.03	−0.48	0.11	−0.06
100	3.54	2.89	−0.56	0.11	−0.07
150	3.45	2.79	−0.62	0.12	−0.07

Here, t, t', and t'' are the nearest, next-nearest, and next-next-nearest neighbor $d_{x^2-y^2}$-hoppings.
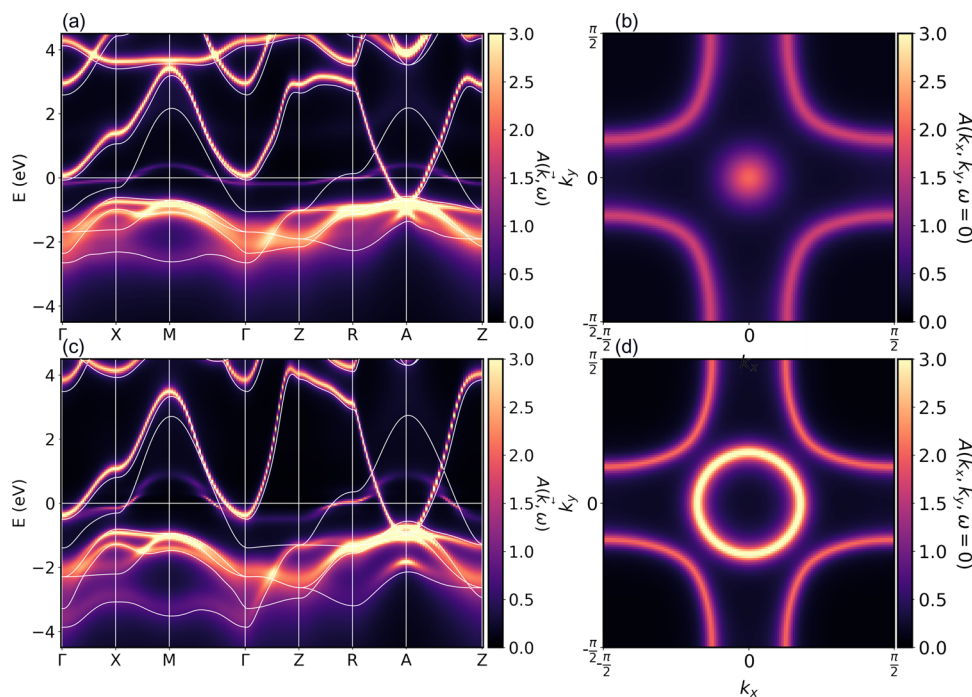
Fig. 2 | Spectral function for undoped PNO. Panels **a** and **c** show the DMFT spectral function $A(\mathbf{k}, \omega)$ (color scale) and the Wannier bands (white lines) along a path through the Brillouin zone at temperature $T = 300K$ and a pressure of 0 and 50 GPa, respectively. Panels (**b**) and (**d**) show the same spectral function in the $k_z = 0$ plane. $A(k_x, k_y, k_z = 0, \omega = 0)$. The Γ point is at the center, i.e., $(k_x = 0, k_y = 0)$.

pocket, on the other hand, mainly hybridizes with other Ni orbitals that, in turn, couple to the Ni $d_{x^2-y^2}$ through Hund's J. Note, however, that the main spectral contribution of these other Ni-d orbitals is still well below the Fermi energy in Fig. 2.

The above justifies a one-band minimal model for super-conductivity in PNO[13,20,29], with the working hypothesis that super-conductivity arises from the correlated Ni $d_{x^2-y^2}$ band only. However, the effective hole-doping δ of the Ni $d_{x^2-y^2}$ band (relative to half-filling) has to be calculated from the 10-band DFT + DMFT to properly account for the electrons in the pockets. In the following, it is thus imperative to always distinguish between the number of holes corresponding to Sr substitution of the Pr site (chemical doping x) and the holes in the Ni $d_{x^2-y^2}$ band compared to half filling (effective doping δ).

The electron pockets induce a nonlinear dependency of δ from x, and their growth with pressure P causes δ to increase by about 0.06 from 0 to 100 GPa, see SM Fig. S7.

Using the effective doping δ of the Ni $d_{x^2-y^2}$ band, we perform a second DMFT calculation for the single Ni $d_{x^2-y^2}$ orbital, which we describe as a single-band Hubbard model with an interaction of $U = 3.4$ eV. This U is smaller than for the 10-band model due to additional screening, but it is notably insensitive to pressure (cf. SM Table S2). The main effect of pressure is instead the increase of t as summarized in Table 1 and the already mentioned enhanced self-doping.

In Fig. 3, we show the spectral function $A(\mathbf{k}, \omega)$ of the 1-band model for PNO as a function of pressure and $x = 0$. The panels for 0 and 50 GPa can be compared to Fig. 2a, c and show that the 1-band model reproduces the renormalization of the Ni $d_{x^2-y^2}$ orbital in the fully-fledged 10-band calculation (see Table S4) for a quantitative comparison.

Hubbard bands are visible at all pressures in Fig. 3, but become more spread out and less defined with increasing pressure. Simultaneously, the effective mass m^* decreases, and the bandwidth widens. Similar results but for the experimentally investigated Sr-doping $x = 0.18$ can be found in SM Fig. S12 and as a function of doping at 50 GPa in Fig. S11.
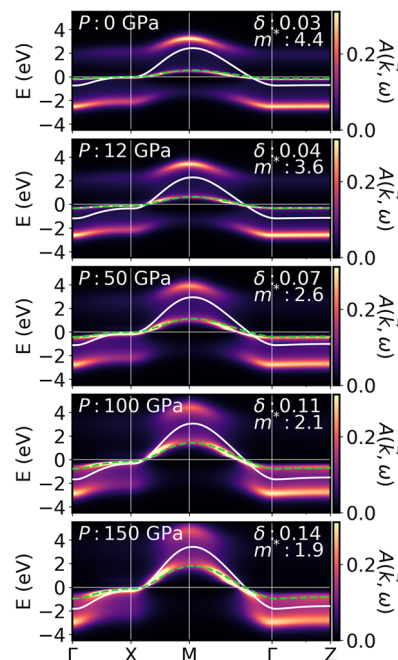

Fig. 3 | DMFT spectral function $A(k_x, k_y, k_z = 0, \omega)$ (color bar) for undoped PNO for the 1-band model and as a function of pressure from 0 to 150 GPa at $T = 0.0125t$. The original DFT Wannier band and the same band renormalized with the effective mass are shown as solid white and dashed green lines, respectively.

Next, we calculate the superconducting T_c using DΓA[35,37]. In Fig. 1, we follow four different paths in parameter space: as a function of doping at (a) 0 GPa and (b) 50 GPa as well as as a function of pressure with Sr-doping (c) $x = 0.18$, i.e., for the parent compound, and (d) $x = 0$. At ambient pressure in Fig. 1a our results are in excellent agreement with our previous calculations for other nickelates[20,29], cf. SM Fig. S14.

The small differences are ascribable to the slightly different material and are in good agreement with experiment[3,27]. We find the effect of pressure to be significant: At 50 GPa, the maximum T_c is enhanced by a factor of two compared to ambient pressure, while the maximum slightly shifts to lower doping ($x = 0.10$). Remarkably, even the undoped parent compound becomes superconducting at 50 GPa [$x = 0$ in Fig. 1b], due to the increased self-doping from the electron pockets.

The experimental Sr-doping of $x = 0.18$[38] is close to optimal doping at 0 GPa. Increasing pressure in Fig. 1c, we observe an increase of T_c by 0.81 K/GPa in excellent agreement with the experimental rate of 0.96 K/GPa[38], for pressures up to 12 GPa. The predicted T_c of 30 K at 0 GPa is slightly higher in theory than the experimental 18 K[38], but still in good agreement. As pressure increases beyond 12 GPa, T_c continues to grow and peaks at around 50 GPa with 49 K, before decreasing for higher pressures.

Most striking is the result for the undoped compound PNO in Fig. 1d. Here, superconductivity sets in below 50 GPa and peaks at almost 100 K around 100 GPa. Intrinsic doping from the electron pockets is sufficient to make the parent compound superconducting at high temperatures.

Discussion

To rationalize our results, we plot the four paths at a fixed pressure, respectively, fixed Sr-doping x in Fig. 4, but now as a function of U/t and the effective hole doping δ of the Ni $d_{x^2-y^2}$ orbital. Superimposed is the DΓA superconducting eigenvalue λ as calculated already in[29], which qualitatively agrees with dynamical cluster (DCA) calculations performed at higher T's[39]. The darker gray regions correspond to a higher T_c. At small dopings we show no superconducting eigenvalue as it competes here with antiferromagnetic order, see, e.g.,[40] and the Supplemental Material.

The application of an isotropic pressure on infinite-layer PrNiO$_2$ has two effects: First, it boosts the hopping t of the Ni $d_{x^2-y^2}$ orbital, which at 150 GPa becomes almost twice as large as at 0 GPa, see Table 1. This increases the overall energy scale and thus enhances T_c. Since U does not change significantly, the ratio U/t also decreases. This is preferable for superconductivity since at ambient pressure PNO exhibits a U/t slightly above the optimum of $U/t \sim 6$ (above the darker gray region in Fig. 4). However, at high pressures of e.g., 100 GPa and 150 GPa curves (c) and (d) have passed the optimum in Fig. 4; T_c in Fig. 1 decreases again.
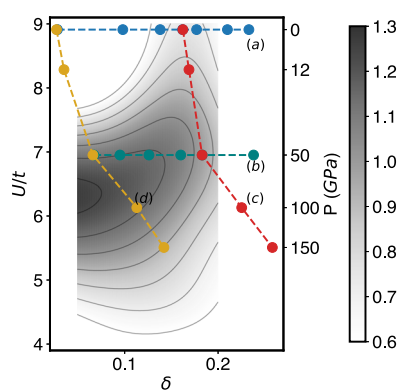

Fig. 4 | Strength of superconductivity with respect to band filling and U/t. The considered four paths in the U/t vs. effective hole doping δ parameter space are: at a fixed pressure of **a** 0 GPa and **b** 50 GPa as a function of Sr-doping x; as a function of pressure for fixed Sr-doping **c** $x = 0.18$ and **d** $x = 0.00$ (blue, green, red, and yellow dots, respectively). The gray color bar and the isocontour lines indicate the strength of superconductivity (superconducting eigenvalue λ at $T = 0.01t$; data from Fig. 3 of ref.[29]). The secondary y-axis reports the pressure corresponding to the U/t values shown.

Second, pressure enhances the effective hole doping δ even at fixed Sr-doping x, as the electron pockets become larger. For this reason, curves (c) and (d) in Fig. 4 deviate from a vertical line. For Sr-doping (c) $x = 0.18$, which is close to optimum at 0 GPa, the curve moves away from optimum doping to the overdoped region when pressure is applied. This is a major driver for the decrease of T_c above 50 GPa in Fig. 1c. In stark contrast, for the parent compound ($x = 0$; d) the effective hole doping δ goes from underdoping to optimal doping, and only at much larger pressures to overdoping and too small U/t. Consequently, PNO without doping hits the sweet spot for superconductivity in Fig. 4 at a pressure between 50 and 100 GPa.

In short, our results strongly suggest that experiments for infinite-layer nickelates are still far from having achieved their maximum T_c. Surprisingly, the maximum T_c of almost 100 K is predicted to be found in undoped PrNiO$_2$ between 50 and 100 GPa. This places nickelates almost on par with cuprates in the Olympus of high-T_c superconductors. The nickelate phase diagram under pressure will not only exhibit a significant increase in T_c but also a wider dome. In particular, the maximum of this dome is shifted to lower Sr-doping x when a pressure of 50–100 GPa is applied.

Such pressures can be achieved experimentally in diamond anvil cells. An alternative route to obtain the same in-plane lattice compression is using a substrate with smaller lattice parameters. For example, LaAlO$_3$, YAlO$_3$, and LuAlO$_3$ have lattice parameters of 3.788[41], 3.722[42], and 3.690 Å[43], respectively, which are already close to the in-plane lattice constants at 50 GPa. As this approach would not change the out-of-plane lattice parameter, the self-doping of the Ni $d_{x^2-y^2}$ band from the electron pockets should be less important. Hence, we expect that with these substrates a higher T_c might be achieved, but only with at least 10% doping.

Methods

In this section, we summarize the computational methods employed. The interested reader can find additional information in Supplementary Material, and data and input files for the whole set of calculations in the associated data repository[44].

Density functional theory calculations were performed using the Vienna ab initio simulation package (VASP)[45,46] using projector-augmented wave pseudopotentials and Perdew-Burke-Ernzerhof exchange-correlation functional adapted for solids (PBESol)[47,48], with a cutoff of 500 eV for the plane wave expansion. Integration over the Brillouin zone was performed over a grid with a uniform spacing of 0.25 Å^{-1} and a Gaussian smearing of 0.05 eV. Wannierization was performed using `wannier90`[49].

The Hubbard U of the 1-orbital setup under pressure was computed from first principles using the constrained random phase approximation (cRPA) in the Wannier basis[50] for entangled band-structures[51] relying on a DFT electronic structure obtained from a full-potential linearized muffin-tin orbital method[52].

DMFT calculations were performed using `w2dynamics`[53], with values of U, J, and t as detailed in the main text and in SM Tables S1 and S3. The 10-band calculations were performed at a temperature of 300 K, with a total of 30 iterations to converge the local Green's function, and a final step with higher sampling. The 1-band DMFT calculations were performed at variable temperatures, with a total of 70 iterations, and a final step with higher sampling, which was increased at lower temperatures. Self-consistency between DMFT and DFT was not considered.

The calculation of the non-local quantities via ladder DΓA is done as before[20] as follows: (1) Starting from the local irreducible particle-hole vertex obtained with `w2dynamics`[54], we calculate non-local susceptibilities and vertices using the `DGApy` code[55]. Here, we calculate the particle-hole ladder and use the Moriya λ correction to mimic self-consistency. (2) The non-local vertices of (1) are fed into the particle-particle channel solving the linearized Eliashberg equation. This is akin

to one parquet step without self-consistency (which would require feeding back the particle–particle corrections to the particle–hole channel). See Supplemental Material for further details and discussions.

Data availability
All the data generated in this study, along with input and output files are available in a repository hosted by TU Wien (see[44]). Related data, including the local Green's functions and DFT calculations are also available in the `NOMAD` repository[56,57].

Code availability
`Quantum ESPRESSO` and `w2dynamics` are publicly available codes. The `DGApy` code employed in this work was also made publicly available at:[55].

References
1. Bednorz, J. G. & Müller, K. A. Possible high-T_c superconductivity in the Ba-La-Cu-O system. *Z. Phys. B Condens. Matter* **64**, 189–193 (1986).
2. Li, D. et al. Superconductivity in an infinite-layer nickelate. *Nature* **572**, 624–627 (2019).
3. Osada, M., Wang, B. Y., Lee, K., Li, D. & Hwang, H. Y. Phase diagram of infinite layer praseodymium nickelate $Pr_{1-x}Sr_xNio_2$ thin films. *Phys. Rev. Mater.* **4**, 121801 (2020).
4. Zeng, S. et al. Phase diagram and superconducting dome of infinite-layer $Nd_{1-x}Sr_xNiO_2$ thin films. *Phys. Rev. Lett.* **125**, 147003 (2020).
5. Zeng, S. et al. Superconductivity in infinite-layer nickelate La1-xCaxNiO2 thin films. *Sci. Adv.* **8**, eabl9927 (2022).
6. Osada, M. et al. Nickelate superconductivity without rare-earth magnetism: (La, Sr)NiO$_2$. *Adv. Mater.* **n/a**, 2104083 (2021).
7. Pan, G. A. et al. Superconductivity in a quintuple-layer square-planar nickelate. *Nat. Mater.* https://doi.org/10.1038/s41563-021-01142-9 (2021).
8. Anisimov, V. I., Bukhvalov, D. & Rice, T. M. Electronic structure of possible nickelate analogs to the cuprates. *Phys. Rev. B* **59**, 7901–7906 (1999).
9. Chow, L. E. & Ariando, A. Infinite-layer nickelate superconductors: a current experimental perspective of the crystal and electronic structures. *Front. Phys.* **10**, 834658 (2022).
10. Meier, Q. N. et al. Preempted phonon-mediated superconductivity in the infinite-layer nickelates. *Phys. Rev. B* **109**, 184505 (2024).
11. Cataldo, S. D., Worm, P., Si, L. & Held, K. Absence of electron-phonon-mediated superconductivity in hydrogen-intercalated nickelates. *Phys. Rev. B* **108**, 174512 (2023).
12. Nomura, Y. et al. Formation of a two-dimensional single-component correlated electron system and band engineering in the nickelate superconductor NdNiO$_2$. *Phys. Rev. B* **100**, 205138 (2019).
13. Held, K. et al. Phase diagram of nickelate superconductors calculated by dynamical vertex approximation. *Front. Phys.* https://www.frontiersin.org/article/10.3389/fphy.2021.810394 (2022).
14. Botana, A. S. & Norman, M. R. Similarities and differences between LaNiO$_2$ and CaCuO$_2$ and implications for superconductivity. *Phys. Rev. X* **10**, 011024 (2020).
15. Wang, Z., Zhang, G.-M., Yang, Y.-f & Zhang, F.-C. Distinct pairing symmetries of superconductivity in infinite-layer nickelates. *Phys. Rev. B* **102**, 220501 (2020).
16. Sakakibara, H. et al. Model construction and a possibility of cuprate-like pairing in a new d^9 nickelate superconductor (Nd, Sr)nio$_2$. *Phys. Rev. Lett.* **125**, 077003 (2020).
17. Wu, X. et al. Robust $d_{x^2-y^2}$-wave superconductivity of infinite-layer nickelates. *Phys. Rev. B* **101**, 060504 (2020).
18. Jiang, P., Si, L., Liao, Z. & Zhong, Z. Electronic structure of rare-earth infinite-layer $RNiO_2$(R = La, Nd). *Phys. Rev. B* **100**, 201106 (2019).
19. Hirayama, M., Tadano, T., Nomura, Y. & Arita, R. Materials design of dynamically stable d^9 layered nickelates. *Phys. Rev. B* **101**, 075107 (2020).
20. Kitatani, M. et al. Nickelate superconductors—a renaissance of the one-band Hubbard model. *npj Quantum Mater.* **5**, 59 (2020).
21. Karp, J. et al. Many-body electronic structure of NdNiO2 and CaCuO2. *Phys. Rev. X* **10**, 021061 (2020).
22. Pascut, G., Cosovanu, L., Haule, K. & Quader, K. F. Correlation-temperature phase diagram of prototypical infinite layer rare earth nickelates. *Commun. Phys.* **6**, 45 (2023).
23. Adhikary, P., Bandyopadhyay, S., Das, T., Dasgupta, I. & Saha-Dasgupta, T. Orbital-selective superconductivity in a two-band model of infinite-layer nickelates. *Phys. Rev. B* **102**, 100501 (2020).
24. Lechermann, F. Late transition metal oxides with infinite-layer structure: nickelates versus cuprates. *Phys. Rev. B* **101**, 081110 (2020).
25. Petocchi, F., Christiansson, V., Nilsson, F., Aryasetiawan, F. & Werner, P. Normal state of nd$_{1-x}$sr$_x$nio$_2$ from self-consistent gw + EDMFT. *Phys. Rev. X* **10**, 041047 (2020).
26. Qin, C., Jiang, M. & Si, L. Effects of different concentrations of topotactic hydrogen impurities on the electronic structure of nickelate superconductors. *Phys. Rev. B* **108**, 155147 (2023).
27. Lee, K. et al. Linear-in-temperature resistivity for optimally superconducting (Nd,Sr)NiO2, *Nature* **619**, 288–292 (2023).
28. Worm, P. et al. Correlations tune the electronic structure of pentalayer nickelates into the superconducting regime. *Phys. Rev. Mater.* **6**, L091801 (2022).
29. Kitatani, M. et al. Optimizing superconductivity: from cuprates via nickelates to palladates. *Phys. Rev. Lett.* **130**, 166002 (2023).
30. Wang, N. N. et al. Pressure-induced monotonic enhancement of T_c to over 30 K in the superconducting Pr$_{0.82}$Sr$_{0.18}$NiO$_2$ thin films. *Nat. Commun.* **13**, 4367 (2022).
31. Christiansson, V., Petocchi, F. & Werner, P. GW + EDMFT investigation of Pr$_{1-x}$Sr$_x$NiO$_2$ under pressure. *Phys. Rev. B* **107**, 045144 (2023).
32. Sun, H. et al. Superconductivity near 80 kelvin in single crystals of La$_3$Ni$_2$O$_7$ under pressure. *Nature* **621**, 493 (2023).
33. Sakakibara, H. et al. Theoretical analysis on the possibility of superconductivity in a trilayer Ruddlesden-Popper nickelate La$_4$Ni$_3$O$_{10}$ under pressure and its experimental examination: comparison with La$_3$Ni$_2$O$_7$. *Phys. Rev. B* **109**, 144511 (2024).
34. Tomczak, J. M., Miyake, T., Sakuma, R. & Aryasetiawan, F. Effective Coulomb interactions in solids under pressure. *Phys. Rev. B* **79**, 235133 (2009).
35. Kitatani, M., Arita, R., Schäfer, T. & Held, K. Strongly correlated superconductivity with long-range spatial fluctuations. *J. Phys.* **5**, 034005 (2022).
36. Si, L. et al. Topotactic hydrogen in nickelate superconductors and akin infinite-layer oxides ABO$_2$. *Phys. Rev. Lett.* **124**, 166402 (2020).
37. Rohringer, G. et al. LadderDΓA code. github.com/ladderDGA (2018).
38. Wang, N. et al. Pressure-induced monotonic enhancement of tc to over 30 k in the superconducting Pr$_{0.82}$Sr$_{0.18}$NiO$_2$ thin films. *Nat. Commun.* **13**, 4367 (2022).
39. Chen, X., LeBlanc, J. P. F. & Gull, E. Superconducting fluctuations in the normal state of the two-dimensional hubbard model. *Phys. Rev. Lett.* **115**, 116402 (2015).
40. Karp, J., Hampel, A. & Millis, A. J. Superconductivity and antiferromagnetism in ndnio$_2$ and CaCuO$_2$: a cluster dmft study. *Phys. Rev. B* **105**, 205131 (2022).
41. Savchenko, V., Ivashkevich, L. & Meleshko, V. Phase transformations in the systems la 2 o 3-a1 2 o 3-mo (m= ni, cu). *Inorg. Mater.* **21**, 1499–1501 (1986).
42. Ismailzade, I., Smolenskii, G., Nesterenko, V. & Agaev, F. X-ray and electric investigations of the systems y (mn1- xbx) o3 (b= fe3+, cr3+, al3+). *Phys. Status Solidi A* **5**, 83–89 (1971).

43. Shishido, T., Nojima, S., Tanaka, M., Horiuchi, H. & Fukuda, T. Flux growth of perovskite-type ralo3 single crystals. *J. Alloy. Compd.* **227**, 175–179 (1995).

44. Additional data related to this publication, including input/output files and raw data for both DFT and DMFT calculations is available at https://doi.org/10.48436/9xych-d8n28.

45. Kresse, G. & Furthmüller, J. Efficient iterative schemes for ab-initio total-energy calculations using a plane-wave basis set. *Phys. Rev. B* **54**, 11169 (1996).

46. Kresse, G. & Furthmüller, J. From ultrasoft pseudopotentials to the projector augmented-wave method. *Phys. Rev. B* **59**, 1758 (1999).

47. Perdew, J. P., Burke, K. & Ernzerhof, M. Generalized gradient approximation made simple. *Phys. Rev. Lett.* **77**, 3865 (1996).

48. Perdew, J. P. et al. Restoring the density-gradient expansion for exchange in solids and surfaces. *Phys. Rev. Lett.* **100**, 136406 (2008).

49. Mostofi, A. A. et al. wannier90: a tool for obtaining maximally-localised wannier functions. *Comput. Phys. Commun.* **178**, 685–699 (2008).

50. Miyake, T. & Aryasetiawan, F. Screened coulomb interaction in the maximally localized wannier basis. *Phys. Rev. B* **77**, 085122 (2008).

51. Miyake, T., Aryasetiawan, F. & Imada, M. Ab initio procedure for constructing effective models of correlated materials with entangled band structure. *Phys. Rev. B* **80**, 155134 (2009).

52. Methfessel, M., van Schilfgaarde, M. & Casali, R. A full-potential lmto method based on smooth hankel functions. *Electron. Struct. Phys. Prop. Solids* **535**, 114–147 (2000).

53. Wallerberger, M. et al. w2dynamics: Local one- and two-particle quantities from dynamical mean field theory. *Comp. Phys. Commun.* **235**, 388 – 399 (2019).

54. Parragh, N., Toschi, A., Held, K. & Sangiovanni, G. Conserved quantities of $su(2)$-invariant interactions for correlated fermions and the advantages for quantum Monte Carlo simulations. *Phys. Rev. B* **86**, 155158 (2012).

55. Worm, P. Dgapy. https://doi.org/10.5281/zenodo.10406493 (2023).

56. https://nomad-lab.eu/prod/v1/gui/user/uploads/upload/id/fRI7D7sdTQOO0f6H_bPPgCg.

57. Scheidgen, M. et al. Nomad: a distributed web-based platform for managing materials science research data. *J. Open Source Softw.* **8**, 5388 (2023).

58. Osada, M. et al. A superconducting praseodymium nickelate with infinite layer structure. *Nano Lett.* **20**, 5735–5740 (2020).

Acknowledgements

Author contributions

S.D.C. performed the DFT and DMFT calculations. S.D.C. and P.W. performed the DΓA calculations. J.M.T. performed the cRPA calculations. L.S. and K.H. designed and supervised the project. All authors participated in the discussion, contributed to the writing of the paper, and approved the submitted version.

Competing interests

The authors declare no competing interests.

Additional information

Supplementary information The online version contains supplementary material available at https://doi.org/10.1038/s41467-024-48169-5.

Correspondence and requests for materials should be addressed to Simone Di Cataldo.

Peer review information *Nature Communications* thanks Antoine Georges, Alexander Hampel and the other, anonymous, reviewer(s) for their contribution to the peer review of this work. A peer review file is available.

Reprints and permissions information is available at http://www.nature.com/reprints

Publisher's note Springer Nature remains neutral with regard to jurisdictional claims in published maps and institutional affiliations.